Nanoscale Res Lett (2010) 5:1706–1711
DOI 10.1007/s11671-010-9729-4

NANO IDEAS

Synthesis of Bio-Compatible SPION–based Aqueous Ferrofluids and Evaluation of RadioFrequency Power Loss for Magnetic Hyperthermia

A. P. Reena Mary · T. N. Narayanan · Vijutha Sunny · D. Sakthikumar · Yasuhiko Yoshida · P. A. Joy · M. R. Anantharaman

Received: 9 May 2010 / Accepted: 2 August 2010 / Published online: 15 August 2010

Abstract Bio-compatible magnetic fluids having high saturation magnetization find immense applications in various biomedical fields. Aqueous ferrofluids of superparamagnetic iron oxide nanoparticles with narrow size distribution, high shelf life and good stability is realized by controlled chemical co-precipitation process. The crystal structure is verified by X-ray diffraction technique. Particle sizes are evaluated by employing Transmission electron microscopy. Room temperature and low-temperature magnetic measurements were carried out with Superconducting Quantum Interference Device. The fluid exhibits good magnetic response even at very high dilution (6.28 mg/cc). This is an advantage for biomedical applications, since only a small amount of iron is to be metabolised by body organs. Magnetic field induced transmission measurements carried out at photon energy of diode laser (670 nm) exhibited excellent linear dichroism. Based on the structural and magnetic measurements, the power loss for the magnetic nanoparticles under study is evaluated over a range of radiofrequencies.

Keywords Superparamagnetism · Magnetic heating · Power loss · Magnetic relaxation · Magnetic hyperthermia

Introduction

Colloidal suspensions of ultrafine magnetic particles (ferrofluids) have widespread applications in fields of both engineering [1–3] and biomedicine [3–6]. Ferrofluids are used in loudspeakers as coolants and dampers, in dynamic sealing, smart Ferrogel preparation [7] for controlled delivery of drugs and as contrast enhancing agents [8]. Ferrofluids are synthesized by dispersing nanosized magnetic particles in carrier liquids with suitable surfactants and proper stabilization techniques. The biocompatibility and the ease with which it can be dispersed in water qualify iron oxide–based ferrofluid a competent candidate for membrane separation, intraocular retinal repair, early diagnosing, imaging and magnetic hyperthermia [9] for cancer therapy, enzyme immobilization of cell targeting and targeted drug delivery [10]. The surface area, size and shape of the nanoparticles decide the physical and chemical properties of these particles to a great extent, which in turn decide the performance in various applications [11]. The particle size, and its distribution, the magnetic and flow properties of the fluid influence the application parameters especially in biomedicine. The spherical shape and monodispersibility of SPIONs are often a prerequisite for application in living tissues [12]. So, optimization of the synthesis of nanoparticles and their conjugation with organic molecules onto the surface becomes very much essential.

A. P. Reena Mary · T. N. Narayanan · V. Sunny · M. R. Anantharaman (✉)
Department of Physics, Cochin University of Science and Technology, Cochin 682022, India
e-mail: mraiyer@yahoo.com

D. Sakthikumar · Y. Yoshida
Bio-Nano Electronics Research Centre, Department of Applied Chemistry, Toyo University, Tokyo, Japan

P. A. Joy
National Chemical Laboratories, Pune, India

Present Address:
T. N. Narayanan
Department of Mechanical Engineering and Materials Science, Rice University, Houston, TX, USA

Magnetic hyperthermia surmounts other techniques of hyperthermia for cancer treatment because of reduced side effects such as damage to healthy tissues [13]. Magnetic hyperthermia or magneto-thermo cytolysis refers to heating of cells attached to magnetic particle by an external AC magnetic field. The increase in temperature is caused due to hysteresis loss. In the case of superparamagnetic particles, the loss is caused by the relaxation processes [14]. The heat dissipated when subjected to an alternating magnetic field depends on the fluid properties such as viscosity, the ratio of relaxation frequency to the applied frequency, size distribution of the magnetic component, domain magnetization and density and the specific heat capacity of the magnetic constituent [15]. There are reports of reduction in magnetization with decrease in particle size in the case of oxide magnetic materials [16]. This is due to finite size effect. Magnetic nanoparticles–drug conjugate attached to an antibody or hormone can be magnetically guided to the tumour site and could specifically bind to it. This provides a platform for optimum dosage of drug.

The stability of the fluid against sedimentation is decided collectively by competing interactions [1, 3, 17, 18] such as van der waals interactions, dipolar interactions, viscous force of the carrier liquid, and the electrostatic and steric repulsion of the surfactant. Surfacted ferrofluid have a long chain of organic molecule around the surface and mainly, steric repulsion provides stabilization. In ionic fluids, the electrostatic repulsion provides stabilization. Hence, the pH of such fluids may vary considerably (from 3 to 9) from basic to acidic depending on the treatment of the nanoparticles after precipitation. Citric acid, a biocompatible surfactant, presents both electrostatic and steric effects and could easily get conjugated to iron oxide particles. Iron oxide is most recommended because of its higher magnetization values, lesser toxicity [19] and the ease of metabolism by the liver. In the present study, we report the synthesis of highly stable water-based iron oxide fluid with narrow particle size distribution at neutral pH, and the evaluation of magnetic properties for hyperthermia application. The cell viability test conducted with these fluids on He La cells was promising (not included). To study the relaxation of the fluid in an external magnetic field, the magneto-optic linear dichroism measurement is presented. The power loss spectrum of these nanoparticles in an external alternating magnetic field is simulated to investigate the possibility of applying in AC magnetic heating.

Experimental

Monodispersed iron oxide particles of average size 9.5 nm were synthesized through controlled chemical co-precipitation method. For this, analytical grade anhydrous ferric chloride ($FeCl_3$) and ferrous sulphate heptahydrate ($FeSO_4.7H_2O$ from Merk) in the molar ratio of 2:1 each in 500 ml of distilled water were taken as the starting solution. To the solution, 12% of aqueous ammonia was added while stirring at room temperature to supersaturate for the precipitation of the oxide. The rate of reaction was controlled by allowing one drop of ammonia per second to react with this solution until a pH of 10, to get a thick dark precipitate. Five grams of citric acid crystals dissolved in 10 ml water was added to this wet precipitate and allowed for further reaction at an elevated temperature of 80°C while stirring for another 90 min. This sample was then washed with distilled water several times for the removal of water soluble byproducts. This is then suspended in distilled water by ultrasound treatment. The obtained fluid was kept for gravity settling of any bare nanoparticles and was then centrifuged at a rotation speed of 3500 rpm to remove any particles that may sediment. The supernatant fluid is extracted for further analysis. The concentration of the magnetic particles is estimated to be 6.28 mg/cc.

The structural characterization was carried out using X-ray diffraction (XRD) technique (Rigaku D Max) at Cu Kα. The particles were analysed with Transmission electron microscopy (TEM). The samples for the above-mentioned experiments were prepared by evaporating the moisture content from the fluid. Room temperature and low temperature magnetic measurements were performed in a Superconducting Quantum Interference Device (SQUID) magnetometer (MPMS Quantum Design). The magneto-optical linear dichroism measurements were carried out on the fluid taken in a 1-cm cuvette at the photon energy of diode laser (670 nm). The simulation of the power loss spectrum of the sample was performed for applied field strength of 500Oe in the range 100–900 kHz.

Results and Discussion

The fluid synthesized exhibited good shelf life and stability against sedimentation under gravitational and magnetic fields. Fluid when an external magnetic field is applied normal to the free surface exhibited good spiking.

Structural and Morphological Analysis

The X-ray diffraction pattern (Fig. 1) shows that the iron oxide particles have crystallized in the inverse spinel structure with a lattice constant of 8.41Å. All the major crystallographic planes corresponding to inverse spinel are identified [ICDD PDF No.750449]. It is hard to differentiate between maghemite (γ Fe_2O_3) and magnetite (Fe_3O_4) using X-ray diffraction analysis alone, since both represent

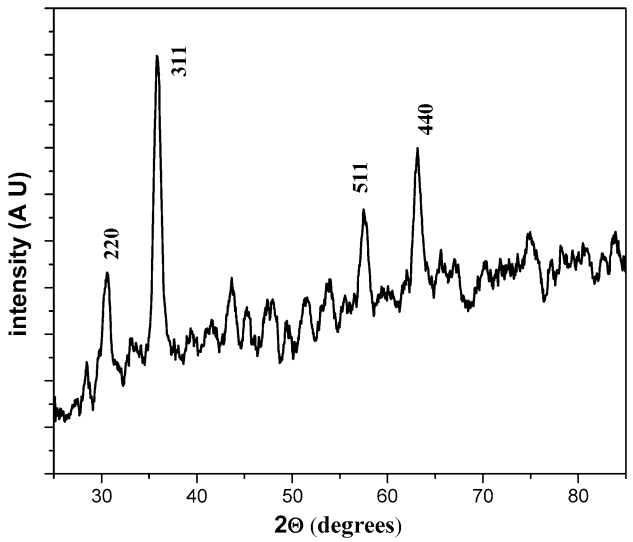

Fig. 1 XRD pattern of the fluid particles

an inverse spinel structure and the (hkl) planes are similar. However, from XRD analysis, it is seen that the compound contains no traces of nonmagnetic haematite (α-Fe_2O_3). There is significant broadening of peaks due to the size reduction in particles. The particle size is calculated from the line broadening applying Scherer's formula [20] and is found to be 9.5 nm. The TEM images (Fig. 2a) show that the particles are nearly spherical. Statistical analysis (Fig. 2b) of the images revealed a normal distribution of particles with a mean size of 10 nm and a width of 3 nm. This is in fair agreement with the particle size obtained from X-ray diffraction measurements.

The narrow size distribution is an advantage while considering the magnetic hyperthermia applications or for targeted drug delivery. The hydrodynamic length of a single citric acid molecule is calculated to be nearly 0.7 nm. This is the thickness of the surfactant monolayer. So, there is a minimum spacing of 1.4 nm between the iron oxide nanoparticles.

Magnetic Characterization

For magnetization measurements, 3 micro litres of the fluid was dropped over to a quartz substrate and the base liquid was allowed to evaporate. Magnetic Hysteresis loops of SPIONs were measured at room temperature and at a low temperature of 6 K and are depicted in Fig. 3. Field-cooled (FC) and zero field–cooled (ZFC) magnetization measurements were carried out in an applied field of 30 mT from 6 to 300 K.

The room temperature M-H loop exhibits negligible coercivity (9Oe) and remanence, which signifies the superparamagnetic nature of particles. This is further verified by fitting experimental curve with the modified Langevin function [21] for the particles with normal size distribution (Fig. 4).

$$M/M_s = L(a), \text{ where a} = \mathrm{mH/k_BT} \quad (1)$$

$$L(a) = Coth(a) - {}^1/_a \quad (2)$$

with normal distribution of particles having a width "***b***" the function get modified to

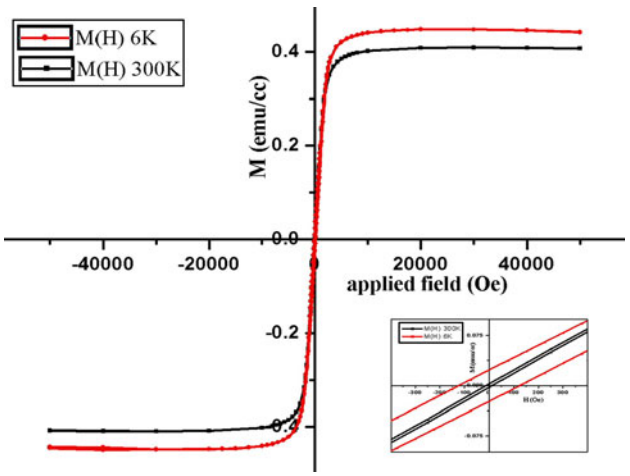

Fig. 3 Magnetic hysteresis curves of SPIONs at 300 and 6 K (*inset*): enlarged loop under low Fields

Fig. 2 **a** Transmission electron micrograph (TEM), **b** particle size distribution

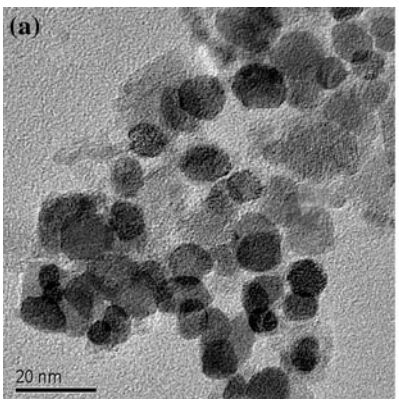

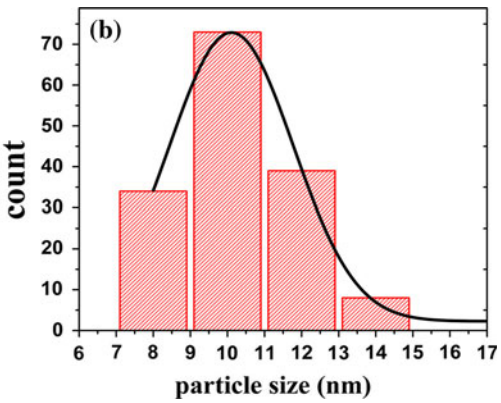

$$L(a) = (1/2ba)\ln\frac{(1-b)\sinh(a(1+b))}{(1+b)\sinh(a(1-b))} \quad (3)$$

Where M is the magnetic moment for an applied field H, M_s is the spontaneous magnetization, k_B is the Boltzmann constant and T the temperature.

At 6 K, the coercivity was 125Oe and where the particles are in a thermodynamically blocked state. This is evident from ZFC measurement also. The saturation magnetization at room temperature calculated by extrapolating the linear portion of Magnetization versus inverse of the applied field at higher field values is 0.418 emu/cc (Fig. 4 (inset). For a concentration of 6.288 mg/cc, the specific magnetization of the magnetic particles is 67emu/g. It is clearly seen that the magnetic moment is saturated at low applied fields and there is no further variation of moment even at high applied fields. If there are any traces of haematite, the moment even at high applied fields would not have been saturated. This is yet another evidence for the nonoccurrence of nonmagnetic iron oxide phase.

The specific magnetization of 67 emu/g for SPIONs is reasonably a good value and is sufficient for applications. The ZFC and FC moments were measured at an applied field of 30mT (Fig. 5). The ZFC shows a broad blocking behaviour with a maximum moment at 140 K, and above this temperature, it decreases gradually. This signifies the distribution of energy barriers present in the sample, and that they act as an ensemble of interacting fine particles. This may be collectively due to the randomly oriented surface spins, the size distribution [22, 23] and the inter-particle interactions. However, the presence of surfactant may eliminate the surface anisotropy as is reported by Roca et al. [24]. The hydrodynamic length of citric acid is nearly 0.7 nm that gives a physical separation of 1.4 nm between

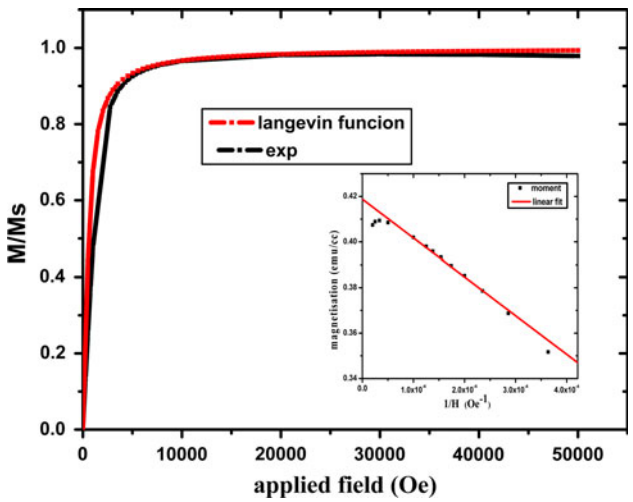

Fig. 4 Theoretical fitting of normalized moment with Langevin function. (*Inset*) Magnetization–H^{-1} plot for Iron Oxide nanoparticles

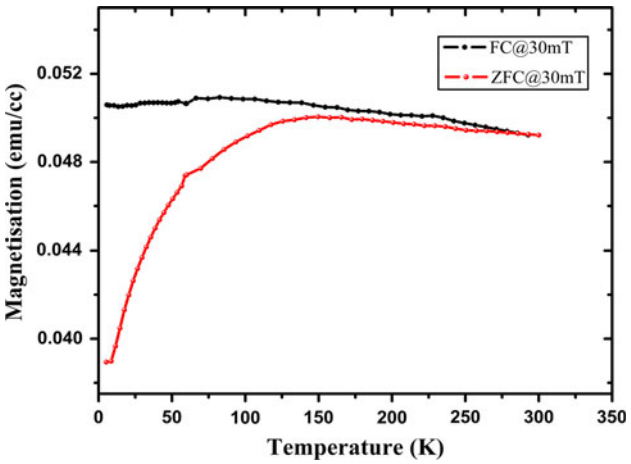

Fig. 5 Zero Field Cooled (ZFC) and Field Cooled (FC) magnetization at 30mT

particles' surfaces, since the base liquid has been dried off before subjecting to magnetization measurements. Thus, there could exist among particles strong dipolar interaction that causes an increase in the effective energy and enhanced magnetic volume. This explains the increased value for the blocking temperature. It is also seen that both the FC and ZFC curves show almost little decrease with temperature which establishes the inter-particle interaction that competes the thermal fluctuation [25].

The interacting nature and hence the enhanced magnetic volume will spoil the performance in biomedical applications. So, to study the actual behaviour of the fluid in an applied magnetic field, magnetic dichroism measurements were carried out.

Magneto-Optical Characterization

Linear magnetic dichroism measurements were carried out on the ferrofluid samples. The linear transmittance was fixed at 10%. The field dependant absorbance of parallel and perpendicular polarized light through magnetized medium is depicted in Fig. 6. Here, the relaxation process has contributions from both Brownian and Neel type.

The absorbance of the light polarized parallel to the applied field increases while that for the perpendicular polarized light decreases, when the field is applied perpendicular to the light propagation. This is expected for a fluid with no preexisting aggregates [26]. Also, it is observed that the transmission relaxes back rapidly to the zero field value as soon as the field is removed. This emphasizes the noninteracting nature of the particles while in the fluid. Citric acid, being ionic in nature, may also contribute to this rapid relaxation since the ions which are diffusing through the system can redistribute the energy faster.

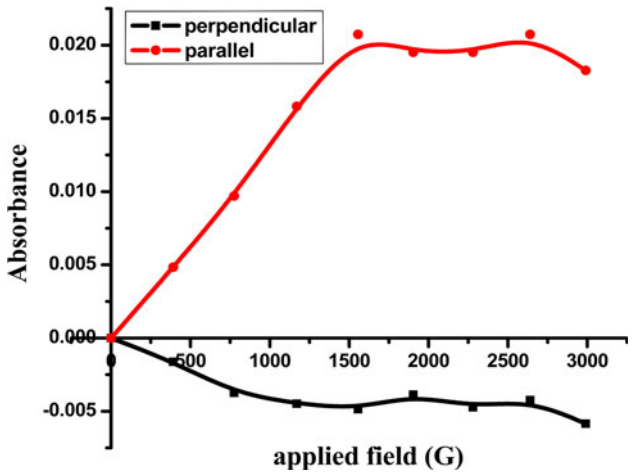

Fig. 6 Field induced optical absorbance for the aqueous ferrofluid in two different polarizations

The superparamagnetic nature, narrow size distribution, noninteracting nature along with high-specific magnetization make this sample a promising candidate for bio-applications. The possibility of this particular sample for magnetic hyperthermia application is analysed theoretically by evaluating the specific power loss in an alternating magnetic field.

Theoretical Analysis for Magnetic Heating

Since the hysteresis is almost negligible as is concluded from M-H loop, the power dissipation is due to the relaxation processes. The power loss produced in an applied AC magnetic field as a function of the relaxation time is given by [27, 28]

$$P = \frac{(mH\omega\tau)^2}{2\tau V k_B T(1+\omega^2\tau^2)} \tag{4}$$

where m is the magnetic moment of the particle, V the particle volume, τ the relaxation time, H is the strength of the magnetic field and ω is the angular frequency of the applied AC magnetic field. The relaxation time τ is given by the equation

$$\frac{1}{\tau} = \frac{1}{\tau_N} + \frac{1}{\tau_B} \tag{5}$$

the Neel relaxation time τ_N is [28]

$$\tau_N = \frac{\sqrt{\pi}\tau_o \exp(KV/k_B T)}{2\sqrt{KV/k_B T}} \tag{6}$$

and the Brownian relation time τ_B is

$$\tau_B = \frac{4\pi\eta r^3}{k_B T} \tag{7}$$

where τ_o is the characteristic time constant $\sim 10^{-9}$s, K the anisotropy constant, η is the viscosity of the medium and r the hydrodynamic radius of the particle. Since the viscosity of living tissue is very high, the Brownian relaxation time becomes very large. So, Neel relaxation dominates when the particle is functionalized and introduced for hyperthermia application. So, the power loss and hence the heat generated becomes a function of domain magnetization, anisotropy and volume of the particle for an AC field of fixed strength and frequency.

The anisotropy constant K is calculated from the relation

$$KV = 25\ k_B T_B \tag{8}$$

where T_B is the blocking temperature obtained from the ZFC measurements. The anisotropic constant calculated is of the same order as that of bulk iron oxide (1.1×10^5 erg/cc) [29] and is closer to the values reported in literature for iron oxide suspended in water [30, 31].

The power loss (also known as specific absorption rate SAR) of the prepared fluid particles, simulated as function of AC frequency in the range of 100–900 kHz, is plotted and is presented in Fig. 7. The results obtained are consistent with the earlier calculations carried out by Okawa et al. [27], where the power loss for varied sizes is evaluated at a noninvasive frequency 120 kHz. Zhang et.al [32] has reported the SAR variation with particle size at still lower frequency of 55 kHz. The applied frequency for maximum power loss depends on the magnetic diameter where the Neel mechanism alone is considered. It is reported that the optimum size for noninvasive frequencies lies around 12–14 nm [27]. Recent simulations [33] show that the power dissipation at an applied frequency of 800 kHz is 80 W/g and for 200 kHz, 10 W/g for an applied field strength of 200 Oe. In this study, the corresponding values of power loss are 330 W/g and 20 W/g, respectively. Li et al. [31] studied the variation of SAR with the

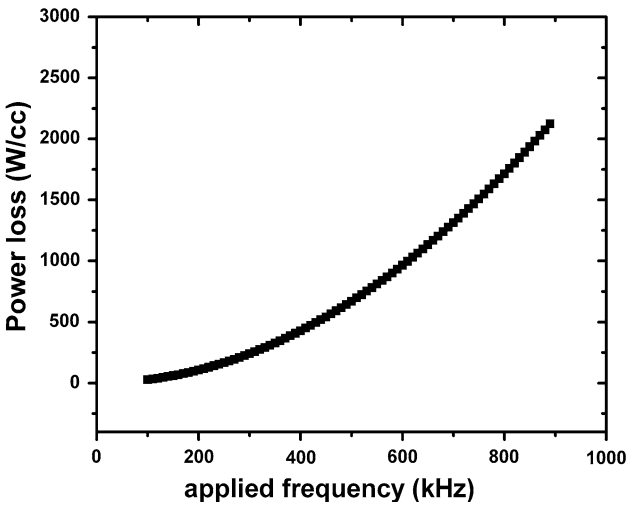

Fig. 7 Power loss spectrum as a function of AC frequency for the ferrofluid

viscosity of the fluid in which an increase in SAR with viscosity was reported till twice the viscosity of water. However, at 55 kHz and 200 Oe, for water suspended fluids, they obtained a power loss of 57 W/g. It is seen from Fig. 7 that the power loss increases with frequency. The optimum frequency for required heat generation could be selected on the basis of the actual experimental condition where magnetic hyperthermia needs to be performed.

Recent studies on cytotoxicity of these ferrofluids indicate that they are highly biocompatible. The cell viability test conducted via well-established 3-(4,5-dimethylthiazole-2-yl)-2,5-diphenyltetrazolium chloride MTT assay [34] on He La cells in vitro shows viability up to a loading of 10 micrograms per ml of cell.

Conclusions

Highly stable aqueous ferrofluid of SPIONs with citric acid as surfactant has been successfully synthesized by controlled chemical co-precipitation method. The structural investigation by XRD and TEM shows good toning in respect of the particle size. The magnetic analysis shows that the nanoparticles are superparamagnetic in nature. The fluid as such is typically a noninteracting ensemble of nanoparticles which is evident from the magneto-optical measurement. The saturation magnetization of the prepared fluid is suitable for various biomedical applications especially for magneto hyperthermia. Based on the magnetic measurements, the power dissipation in an alternating magnetic field of 500 gauss as a function of applied frequency is calculated.

Acknowledgments Authors thank Dr. Ildico Guhr and Prof. G. Schatz University of Konstanz for SQUID measurements, and DST-DAAD personnel exchange programme. MRA thanks AICTE sponsored project "Center for Ferrofluids". RMAP (ID.379) and TNN (ID: 434) acknowledge CSIR and VS thanks UGC RFSMS for research fellowships.

References

1. R.E. Rosensweig, *Ferrohydrodynamics* (Cambridge University Press, New York, 1985)
2. R.P. Castillejos, J.A. Plaza, J. Esteve, P. Losantos, M.C. Acero, C. Cane, F. Serra-Mestres, Sens Actuators **84**, 176 (2000)
3. C. Scherer, A. Figero, M. Neto, Braz. J. Phys **35**(3), 718 (2005)
4. D.K. Kim, M. Mikhaylova, F.H. Wang, J. Kehr, B. Bjelke, Y. Zhang, T. Tsakalakos, M. Muhammed, Chem. Mater. **15**, 4343 (2003)
5. N.A. Brusnetsov, V.V. Gogosov, T.N. Brusnetsova, A.V. Sergeev, N.Y. Jurchenko, A. Kuznetsov, O.A. Kuznetsov, L.I. Shumakov, J. Magn. Magn. Mater. **225**, 113 (2001)
6. D.L. Holligan, G.T. Gillies, J.P. Dailey, Nanotechnology **14**, 661 (2003)
7. T.Y. Liu, S.H. Hu, T.Y. Liu, D. Liu, S.Y. Chen, Langmuir **22**, 5974 (2006)
8. J.F. Lutz, S. Stiller, A. Hoth, L. Kaufner, U. Pison, R. Cartier, Biomacromolecules **7**, 3132 (2006)
9. C.C. Berry, A.S.G. Curtis, J. Phys. D Appl. Phys. **36**, R198 (2003)
10. M. Babincova, V. Altanerova, C. Altaner, C. Bergeman, P. Babinec, IEEE Trans. Nanobioscience **7**, 15 (2008)
11. P. Tartaj, M.P. Morales, S. Veintemillas-Verdaguer, T. Gonzalez-Carreno, C.J. Serna, J. Phys. D Appl. Phys. **36**, R182 (2003)
12. A. Petri-Fink, H. Hofmann, IEEE Trans. Nanobioscience **6**(4), 289 (2007)
13. Q.A. Pankhurst, J. Connolly, S.K. Jones, J. Dobson, J. Phys. D Appl. Phys. **36**, R167 (2003)
14. R. Hiergeist, W. Andrä, N. Buske, R. Hergt, I. Hilger, U. Richter, W. Kaiser, J Magn.Magn.Mater. **201**, 420 (1999)
15. J. Giri, P. Pradhan, T. Sriharsha, D. Bahadur, J. Appl. Phys **97**, 10Q916 (2005)
16. Y. Jun, J. Seo, J. Cheon, Acc. Chem. Res. **41**, 179 (2008)
17. E. Dubois, V. Cabuil, F. Boue, R. Perzynski, J. Chem. Phys. **111**, 7147 (2001)
18. J. de Vincente, A.V. Delgado, R.C. Plaza, J.D.G. Duran, F. Gonsalez-Caballero, Langmuir **16**, 7954 (2000)
19. L.F. Pavon, O.K. Okamoto, Einstein **5**, 74 (2007)
20. B.D. Cullity, S.R. Stock, *Elements of X-ray diffraction* (Prentice Hall, New Jersey, 2001)
21. T.N. Narayanan, A.P. Reena Mary, M.M. Shajumon, L. Ci, P.M. Ajayan, M.R. Anantharaman, Nanotechnology **20**, 055607 (2009)
22. S.J. Lee, J.R. Jeong, S.C. Shin, J.C. Kim, J.D. Kim, J. Magn. Magn. Mater. **282**, 147 (2004)
23. X. Battle, A. Labarta, J. Phys. D Appl. Phys. **35**, R15 (2002)
24. A.G. Roca, M.P. Morales, K. O'Grandy, C.J. Serna, Nanotechnology **17**, 2783 (2006)
25. J. Dai, J.Q. Wang, C. Sangregorio, J. Fang, E. Carpenter, J. Tang, J. Appl. Phys. **87**, 7397 (2000)
26. Q. Zhang, J. Wang, H. Zhu, J.Appl.Phys. **78**, 3999 (1995)
27. K. Okawa, M. Sekine, M. Maeda, M. Tada, M. Abe, N. Matsushida, K. Nishio, H. Handa, J. Appl. Phys **99**, 08102 (2006)
28. R.E. Rosenswieg, J. Magn. Magn. Mater **252**, 370 (2002)
29. B.D. Cullity, *Introduction to Magnetic materials Philippines* (Addison Wesley, London, 1972)
30. Y.Z. Li, C.G. Hong, M.W. Xu, J. Magn. Magn. Mater **311**, 228–233 (2007)
31. M. Ma, Y. Wu, J. Zhou, Y. Sun, Y. Zhang, N. Gu, J. Magn. Magn. Mater. **268**, 33 (2004)
32. L.Y. Zhang, Y.H. Dou, L. Zhang, H.C. Gu, Chin. Phys. Lett. **24**, 483 (2007)
33. S. Purushotham, R.V. Ramanujan, J. Appl. Phys. **107**, 114701 (2010)
34. R. Gopikrishnan, K. Zhang, P. Ravichandran, S. Baluchamy, V. Ramesh, S. Biradar, P. Ramesh, J. Pradhan, J.C. Hall, A.K. Pradhan, G.T. Ramesh, Nano-Micro Lett. **2**, 27–30 (2010)